A closed-form solution of dowel action based on beam on elastic foundation theory and fracture mechanics

Lu, Jiandong; Yang, Yuguang; Hendriks, Max A.N.

DOI
10.1016/j.engstruct.2024.118430

Publication date
2024

Document Version
Final published version

Published in
Engineering Structures

Engineering Structures 315 (2024) 118430

Contents lists available at ScienceDirect

Engineering Structures

journal homepage: www.elsevier.com/locate/engstruct

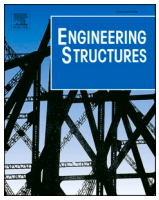

A closed-form solution of dowel action based on beam on elastic foundation theory and fracture mechanics

Jiandong Lu [a,*], Yuguang Yang [a], Max A.N. Hendriks [a,b]

[a] Deparment of Engineering Structures, Delft University of Technology, Stevinweg 1, Delft 2628CN, the Netherlands
[b] Department of Structural Engineering, Norwegian University of Science and Technology, Richard Birkelands vei 1A, Trondheim 7491, Norway

ARTICLE INFO

Keywords:
Dowel action
Unstable dowel splitting
Fracture mechanics
Beam on elastic foundation theory
Critical shear displacement theory

ABSTRACT

This paper proposes a new mechanical model to describe the dowel action with the aim of using the model to gain a deeper understanding of the unstable dowel splitting cracking observed in shear experiments of beams without shear reinforcement. The model was developed by combining beam on elastic foundation (BEF) theory and fracture mechanics. The proposed model is able to predict the whole evolution process of dowel action until the propagation of the dowel splitting crack becomes unstable. The model theoretically proves that the development of a dowel splitting crack can become unstable under certain conditions, therefore leading to the unstable shear failure of the whole member. In addition to the derivation of the analytical model, the paper also validates the model using data from the literature. Finally, an analytical solution of the critical shear displacement that triggers the unstable dowel splitting crack is derived. It can be used to improve the failure criterion initially proposed in the Critical Shear Displacement Theory (CSDT).

1. Introduction

Dowel action is recognized as one of the primary shear transfer mechanisms by many researchers [1–9]. It stands for the mechanism that reinforcement transfers shear force perpendicular to its axial direction. As a shear transfer mechanism, it was first reported by Friberg [10]. In 1965, Acharya and Kemp [11] emphasized the importance of dowel action in the reinforced beam without shear reinforcement.

Various studies in literature [12–15] suggest that dowel action typically contributes 15 %− 25 % of the total shear resistance of a reinforced concrete (RC) beam without shear reinforcement. Therefore, it was not regarded as the most critical shear transfer mechanism. However, Chana [16] found in his shear tests that the width of the dowel crack increased rapidly as the specimens reached the flexural-shear failure. This observation implied that flexural-shear failure is associated with dowel splitting. He also demonstrated that the shear capacity of an RC member could be increased significantly if the dowel splitting is limited by providing additional 'links' locally along the longitudinal reinforcement. A similar observation and conclusion can be found in the test done by Kim and White [17]. Fischer and König [18] pointed out that the failure of dowel action is a necessary and sufficient condition for the flexural-shear failure based on their numerical simulation. Further developed from these observations, Yang [6,9] concluded that unstable dowel splitting triggered the flexural-shear failure based on the energy balance of the whole system and proposed the Critical Shear Displacement Theory (CSDT). The CSDT further assumes that unstable dowel splitting occurs when the vertical shear displacement along a flexural crack reaches a critical value. Therefore, it uses the critical shear displacement as the failure criterion. These models suggest that despite its limited contribution to the total shear resistance, in-depth understanding and modelling of dowel cracking is essential to model the shear failure process of RC members without shear reinforcement.

Several empirical and mechanical models have been proposed in literature based on experimental observations dedicated to dowel action [7,8,15,19–23]. A brief summary of these models is given here. Krefeld and Thurston [19] proposed a novel block-type beam experiment, as shown in Fig. 1(a), to achieve this goal and eliminate the contribution of aggregate interlock. They proposed, based on the observation in the experiments, an empirical equation and concluded that the ultimate capacity of dowel action was related to the distance between the crack initiation point and the support, the beam height, the beam width, the concrete compressive strength, the concrete cover, and the rebar diameter. Taylor [15] and Baumann & Rüsch [24] used a similar test setup to further investigate dowel splitting. However, they reported two

* Corresponding author.
E-mail address: J.Lu-1@tudelft.nl (J. Lu).

https://doi.org/10.1016/j.engstruct.2024.118430
Received 16 February 2024; Received in revised form 15 May 2024; Accepted 9 June 2024
Available online 20 June 2024

different types of load-displacement curves. Taylor [15] reported a post-peak softening behaviour, while Baumann & Rüsch's [24] results showed a nearly perfect elastoplastic curve for dowel splitting failure.

Autrup et al. [7] carried out an experiment using the improved block-type beam experiment, as shown in Fig. 1(b), to further investigate the influence of axial force on dowel splitting. The results they reported were similar to the perfect elastoplastic behaviour when the axial force is relatively low. Nevertheless, the recent experimental data reported by de Resende et al. [8] showed a clear post-peak softening behaviour for the specimens made of conventional concrete. Fig. 2 schematically summarizes the three different responses observed in literature. They show contradictory results, accordingly, no consistent model is available to describe the dowel splitting yet. Additionally, most of the existing available models are aiming at predicting the maximum dowel resistance, the mechanical behaviour after the fracture of concrete is not considered in these models. Consequently, a relationship between dowel resistance and vertical displacement and cracking opening is not well-established, which is crucial to evaluate the shear capacity of RC beams without shear reinforcement using kinematic-based models, Critical Shear Crack Theory (CSCT) [25,26], Critical Shear Displacement Theory (CSDT) [6,9], Shear Crack Propagation Theory (SCPT) [5], etc.

This paper introduces the nonlinear tension softening behaviour of concrete described by concrete fracture mechanics into the Beam on Elastic Foundation (BEF) theory. Different from the plasticity-based BEF theories which are mostly focused on force equilibrium and ultimate limit state, the proposed model can provide the full load-deformation evolution of the dowel action considering the nonlinear behaviour of concrete. The proposed model is further validated with experimental data from the literature, both in ultimate strength and deformation.

2. Proposed mechanical model for dowel action

The model proposed in this paper distinguishes the propagation process of a dowel splitting crack along a longitudinal rebar into three stages, namely the elastic stage before cracking, stable dowel cracking and unstable dowel cracking. This is based on the observation of the propagation process of a dowel crack in literature. In each stage, corresponding models based on the equilibrium conditions along the longitudinal rebar and the material constitutive models are established.

2.1. Elastic stage before cracking

In the elastic stage, the force equilibrium conditions along the longitudinal reinforcement are established using the BEF theory. Following the theory, the reinforcement is treated as a beam placed on an elastic foundation, as shown in Fig. 3. We further assume that it is a semi-infinite long beam in the longitudinal direction to obtain a more compact analytical solution. This assumption is based on the fact that the distance between the initial dowel cracking point and the support is

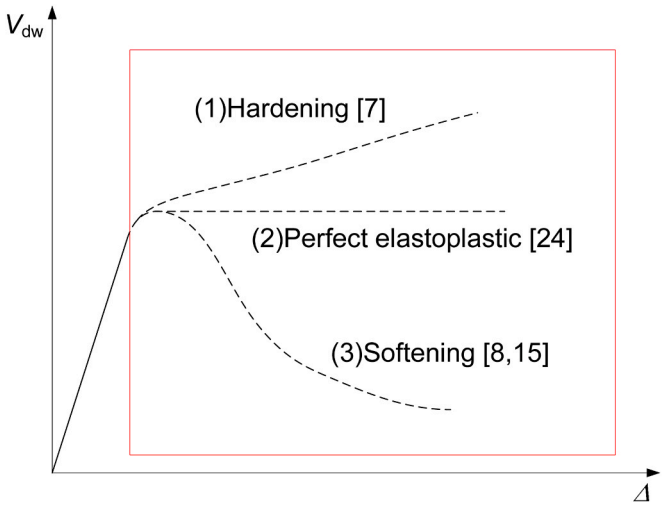

Fig. 2. Schematic illustration for different relationships between dowel force and vertical displacement observed in literature [7,8,15,24].

sufficiently long for a slender beam. It is valid following Marcus' statement [27] that the cracking load for dowel action is not significantly affected by the embedded length of the rebar if the rebar is longer than eight times of rebar diameter. The influence of the beam length is further discussed in Section 4.2.

We further use the solution suggested by Hetényi [28] on a semi-infinite long beam subjected to a concentrated force V_{dw} at the free end as shown in Fig. 3. The dowel force V_{dw} per rebar is defined as V_{dw}/n, with n is the number of rebars. The dowel force is applied at the free end of each rebar. According to Hetényi [28], with a given V_{dw}/n, the longitudinal distributions of vertical displacement u_z, rotation θ, moment M, and shear force V along the rebar can be expressed using Eq. (1)~(4):

$$u_z(x) = \frac{2\lambda V_{dw}}{kn} e^{-\lambda x} \cos \lambda x \tag{1}$$

$$\theta(x) = \frac{2\lambda^2 V_{dw}}{kn} e^{-\lambda x} \left(\cos \lambda x + \sin \lambda x \right) \tag{2}$$

$$M(x) = -\frac{V_{dw}}{\lambda n} e^{-\lambda x} \sin \lambda x \tag{3}$$

$$V(x) = -\frac{V_{dw}}{n} e^{-\lambda x} \left(\cos \lambda x - \sin \lambda x \right) \tag{4}$$

$$\lambda = \sqrt[4]{\frac{k}{4E_s I_s}} = \sqrt[4]{\frac{\phi k_f}{4E_s I_s}} \tag{5}$$

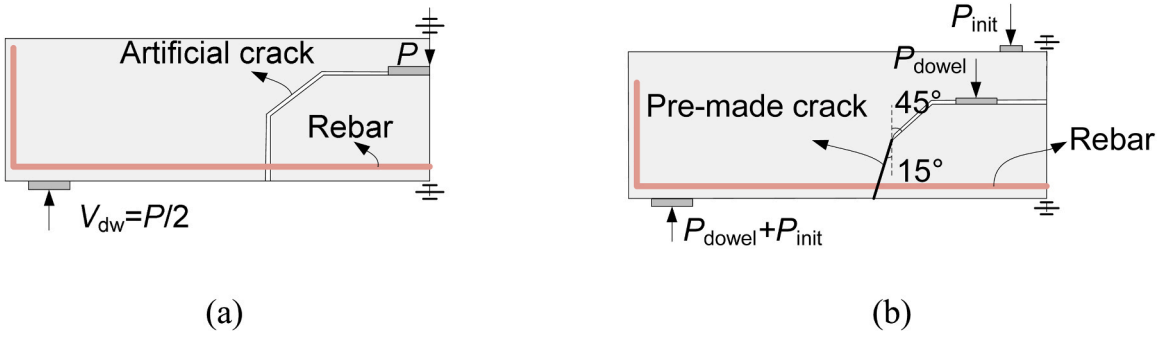

Fig. 1. Block-type test setup for testing dowel action: (a) the setup used by Krefeld and Thurston, reproduced from [19]; (b) the setup used by Autrup et al. reproduced from [7].

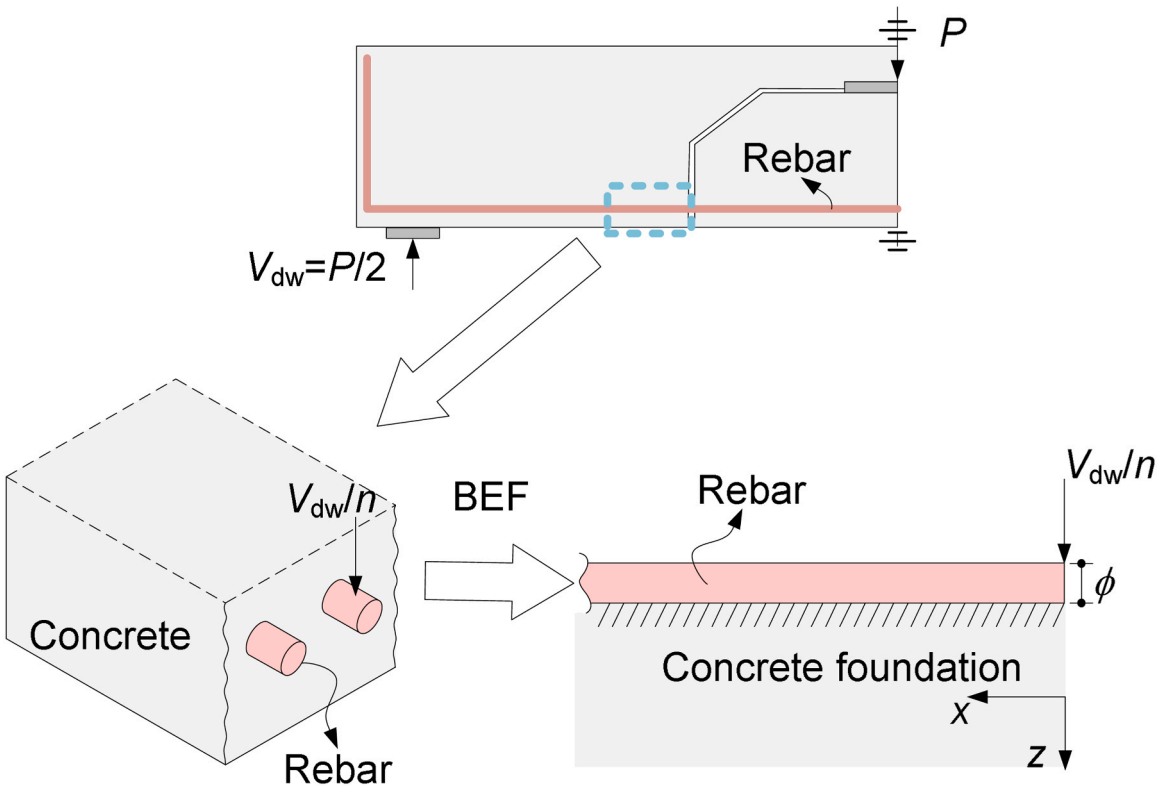

Fig. 3. Schematic drawing of dowel action based on Beam on Elastic Foundation Theory.

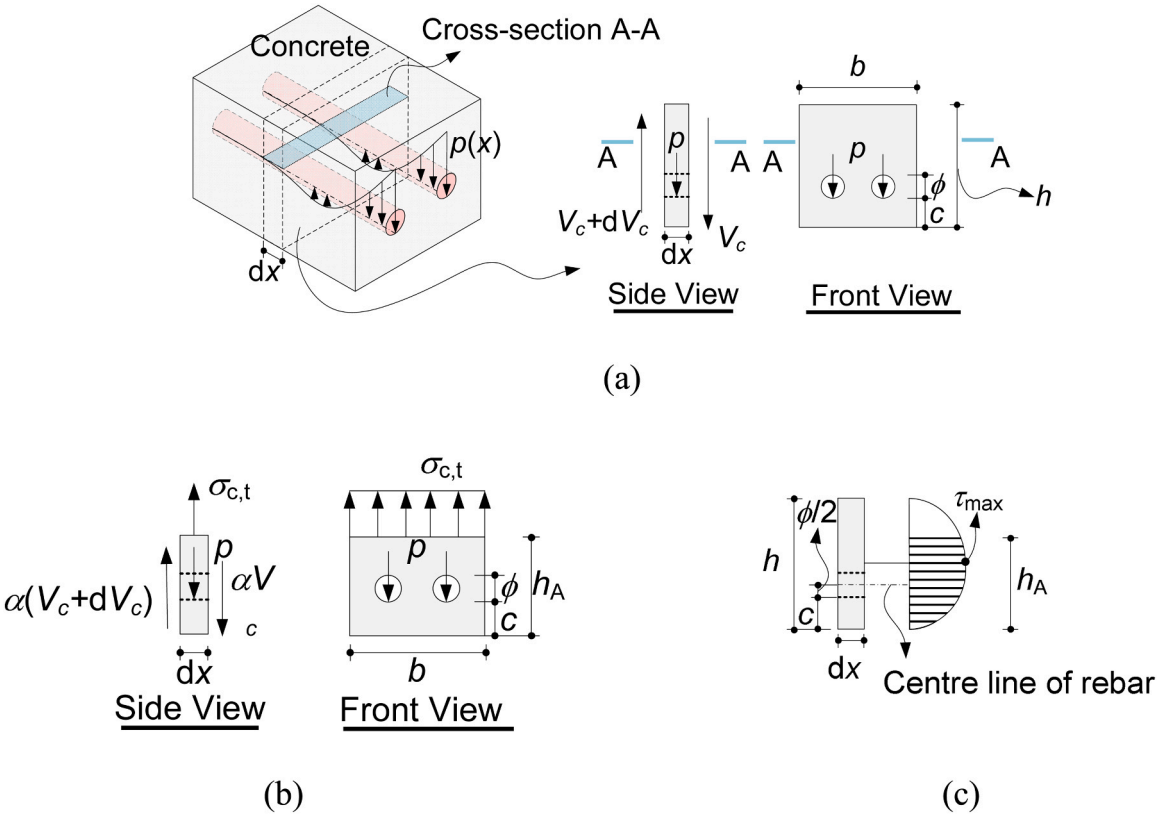

Fig. 4. Illustration for the derivation of equilibrium equation: (a) free body diagram of an infinitesimal element in the longitudinal direction; (b) cross-sectional analysis at an arbitrary section A-A for transversal distribution of concrete stress; (c) assumed shear stress distribution along the height.

where λ is the characteristic value of the beam system, $1/\lambda$ is called characteristic length, x is the distance along the beam starting from the free end, ϕ is the rebar diameter, k_f is the foundation modulus in pressure per length, E_s is Young's module of reinforcement, n is the number of rebars and $I_s = \pi\phi^4/64$ is the moment of inertia of an individual rebar.

The empirical equation proposed by Soroushian et.al [23] is used in this paper to determine the distributed stiffness of the concrete foundation k_f in N/mm^3:

$$k_f = 127 c_f \sqrt{f_c} (1/\phi)^{2/3} \tag{6}$$

Where c_f is an empirical coefficient ranging from 0.6 to 1.0, and f_c is the concrete compressive strength in MPa and ϕ is in mm. In this paper, the c_f was adopted as 0.6 for multiple rebar situations and 1 for single rebar situations.

After determining the material properties, with a given dowel force V_{dw}, the distribution of vertical displacement u_z along the rebar can be calculated using Eq. (1). Then, the vertical reaction force distribution p caused by a single rebar in the concrete foundation can be calculated by:

$$p(x) = k u_z(x) = 2\lambda \frac{V_{dw}}{n} e^{-\lambda x} \cos \lambda x \tag{7}$$

If the action of rebar is replaced by the vertical force distribution on the concrete p, as shown in Fig. 4(a), an infinitesimal element of the concrete part along the longitudinal direction is selected for further analysis. Based on the vertical force equilibrium, the following equation can be derived:

$$dV_c = np(x)dx \tag{8}$$

where V_c is the shear force carried out by the selected concrete cross-section.

Then, an arbitrary cross-section A-A along the height direction is selected to further examine the internal force in concrete, as shown in Fig. 4(b). To simplify the derivation, the concrete stress distribution σ_{ct} in the cross-section A-A is assumed to be uniform along the width direction of the member. The assumption implied behind this statement is in fact the failure mode during the dowel cracking process. As shown by Vintzeleou and Tassios [20], two failure modes – bottom and side splitting can be observed in dowel splitting failure. The bar spacing is one of parameters which can affect the failure mode. However, there is no clear quantitative criterion of bar spacing to distinguish these two failure modes in literature. The adopted assumption in this paper can be only used for side splitting failure. Based on this assumption, the following equation can be derived based on the vertical force equilibrium:

$$b\sigma_{ct}dx = np(x)dx - \alpha dV_c \tag{9}$$

where b is the width of the beam, σ_{ct} is concrete tensile stress in the width direction at a certain height and α is a factor indicating shear force carried by the partial concrete cross-section.

The factor α is obtained by assuming that the shear stress in the concrete cross-section follows a parabolic-shape distribution along the height with the maximum value at the middle height, as shown in Fig. 4 (c). Therefore, the factor α can be represented by the ratio between the shadow area and the total area enclosed by the shear stress distribution. For a rectangular cross-section, the factor can be calculated in the following equation:

$$\alpha = \frac{\int_0^{h_A} -\frac{4\tau_{max}}{h^2}\left(s^2 - hs\right)ds}{\int_0^{h} -\frac{4\tau_{max}}{h^2}\left(s^2 - hs\right)ds} = \frac{3hh_A^2 - 2h_A^3}{h^3} \tag{10}$$

where h_A is the vertical distance between a certain cross-section and the bottom of the cross-section and τ_{max} is the maximum shear stress at the middle height.

Substituting Eqs. (7), (8) and (10) into Eq. (9), the distribution of concrete stress σ_{ct} along the width direction can be expressed by the following equation:

$$\sigma_{ct} = \frac{(1-\alpha)np(x)}{b(h_A)} \tag{11}$$

If different combinations of x and h_A are examined, one may find that the maximum concrete transversal stress $\sigma_{ct,max}$ is reached when $x = 0$ and $h_A = c + \phi/2$, because the vertical reaction force p reaches the maximum value and the cross-section width is minimum. Then, Eq. (11) can be further simplified as follows:

$$\sigma_{ct,\,max} = \left(1 - \alpha_{crit}\right)\frac{2\lambda V_{dw}}{b_n} \tag{12}$$

where $b_n = b - n\phi$ is the net width of the beam, α_{crit} can be calculated using Eq. (13). It should be noted that α in the rest of the following derivation refers to the α_{crit} for simplicity.

$$\alpha_{crit} = 3\left(\frac{c + \phi/2}{h}\right)^2 - 2\left(\frac{c + \phi/2}{h}\right)^3 \tag{13}$$

Finally, by assuming the dowel splitting crack occurs when $\sigma_{ct,max}$ reaches the concrete tensile strength f_{ct}, the dowel cracking load $V_{dw,cr}$ can be derived using the following equation:

$$V_{dw,cr} = \frac{1}{(1-\alpha)}\frac{b_n f_{ct}}{2\lambda} \tag{14}$$

Substituting Eq. (14) into (1), the cracking displacement at the free end $u_{z,cr}$ can be obtained:

$$u_{z,cr} = \frac{1}{(1-\alpha)}\frac{b_n f_{ct}}{nk} \tag{15}$$

Then, the relationship between dowel resistance V_{dw} and vertical displacement $u_{z,max}$ at the free end before cracking can be described using the following linear equation:

$$V_{dw} = \frac{u_{z,\,max}}{u_{z,cr}}\frac{1}{(1-\alpha)}\frac{b_n f_{ct}}{2\lambda} \quad u_z \le u_{z,cr} \tag{16}$$

2.2. Stable dowel cracking

After the dowel splitting crack occurs, the whole system can be divided into two parts by the point of the crack tip: the uncracked part and the cracked part, as shown in Fig. 5. The uncracked part can still be treated using BEF theory. However, it should be noted that a moment M_{tip} should be applied to the crack tip point (the new free end of the BEF model) in addition to a concentrated force V_{tip}. The cracked part, on the other hand, can be simplified as a cantilever beam subjected to the externally applied dowel force V_{dw} and the residual tension stress σ_{res} in the fracture progress zone (FPZ). The length of the cantilever beam equals the total length of the dowel crack L_{dw}. The cantilever beam has an initial vertical rigid movement $u_{z,tip}$ and rotation θ_{tip} and it is in fact a composite beam consisting of both concrete and rebars.

2.2.1. Equilibrium in the uncracked part

The equilibrium conditions in the uncracked part are examined first. The analytical solutions for a semi-infinite beam discussed in the first stage are extended to include the influence of a concentrated moment at the free end according to [28]. The vertical displacement $u_{z,tip}$ and the rotation θ_{tip} at the crack tip are as follows:

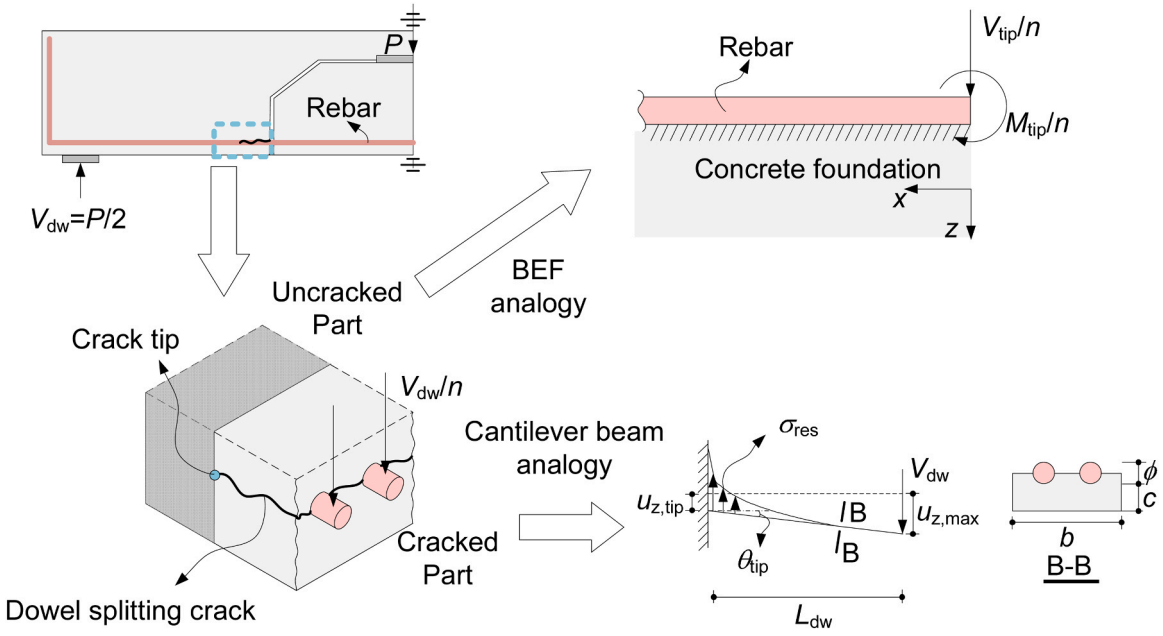

Fig. 5. Proposed mechanical model after dowel splitting cracking.

$$u_{z,tip} = \frac{2\lambda}{k}\frac{V_{tip}}{n} + \frac{2\lambda^2}{k}\frac{M_{tip}}{n} \tag{17}$$

$$\theta_{tip} = \frac{2\lambda^2}{k}\frac{V_{tip}}{n} + \frac{4\lambda^3}{k}\frac{M_{tip}}{n} \tag{18}$$

where V_{tip} and M_{tip} are the concentrated force and moment acting on the crack tip.

Considering that the dowel crack is driven to propagate further, the maximum concrete transversal stress $\sigma_{ct,max}$ at the crack tip shall satisfy the following conditions based on the BEF theory.

$$\sigma_{ct,\,max} = \frac{(1-\alpha)}{b_n} nk u_{y,tip} = (1-\alpha)\frac{2\lambda\left(V_{tip} + \lambda M_{tip}\right)}{b_n} = f_{ct} \tag{19}$$

Using Eq. (19) to further simplify Eqs. (17) and (18), the following expressions can be obtained.

$$u_{z,tip} = \frac{1}{(1-\alpha)}\frac{f_{ct} b_n}{kn} = u_{z,cr} \tag{20}$$

$$\theta_{tip} = \frac{2(1-\alpha)\lambda^3 M_{tip} + \lambda f_{ct} b_n}{(1-\alpha)kn} \tag{21}$$

It turns out that the vertical displacement at the crack tip $u_{z,tip}$ always equals the dowel cracking displacement $u_{z,cr}$ and is a constant depending on the material properties, while the rotation θ_{tip} can be determined only after knowing the moment applied at the crack tip M_{tip}.

2.2.2. Equilibrium in the cracked part

In the cracked part, the main unknown variable is the distribution of the residual tensile stress σ_{res} in the FPZ. The simple power law relationship between residual tensile stress and crack width proposed by Reinhardt [29] is used in this paper:

$$\sigma_{res} = f_{ct}\left(1 - \left(\frac{w}{w_c}\right)^{c_1}\right) \geq 0 \tag{22}$$

where w is the crack width, $c_1 = 0.31$ is an empirical coefficient, $w_c = G_f/f_{ct}\cdot(1+c_1)/c_1$ is the characteristic crack width that can transfer the residual strength and G_f is the fracture energy of concrete, which can be calculated using $G_f = 0.073 f_c^{0.18}$ (G_f is in N/mm and f_c is in MPa) according to *fib* Model Code 2010 [30]. Fig. 5 shows how the force and moment equilibrium of the cracked part are established:

$$V_{tip} = V_{dw} - b_n \int_0^{L_{dw}} \sigma_{res} dx \tag{23}$$

$$M_{tip} = V_{dw} L_{dw} - b_n \int_0^{L_{dw}} \sigma_{res} x dx \tag{24}$$

The residual tensile stress σ_{res} expressed by Eq. (22) depends on the crack width distribution along the cracked part. The crack width along the cracked part is assumed to follow a linear distribution, thus we ignore the elastic deformation of the cracked part because of the large moment inertia of the composite cross-section in the cracked part with respect to the low magnitude of dowel force. This assumption satisfies the experimental observations in some recently published work [7,8]. With this assumption, the crack width distribution w along the cracked part can be described using the rotation θ_{tip} at the crack tip.

$$w = \theta_{tip} x \tag{25}$$

Considering the geometric condition shown in Fig. 5, the maximum crack width w_{max} is expressed by the following expression:

$$w_{max} = u_{z,\,max} - u_{z,cr} \tag{26}$$

where $u_{z,max}$ is the vertical displacement at the free end of the cracked part.

Substituting Eqs. (20), (21) and (26) into Eq. (25), the length of dowel crack L_{dw} can be expressed by the following equation:

$$L_{dw} = \frac{w_{max}}{\theta_{tip}} = \frac{(1-\alpha)knu_{z,\,max} - f_{ct} b_n}{2(1-\alpha)\lambda^3 M_{tip} + \lambda f_{ct} b_n} \tag{27}$$

Combing Eqs. (19), (22), (23) and (24), a closed-form analytical equation for M_{tip} can be derived:

$$M_{\text{tip}} = \begin{cases} \dfrac{f_{\text{ct}} b_{\text{n}} L_{\text{dw}}}{2(1-\alpha)\lambda(1+\lambda L_{\text{dw}})} + \dfrac{f_{\text{ct}} b_{\text{n}} L_{\text{dw}}^2 \left[\dfrac{1}{2} - \dfrac{1}{(1+c_1)(2+c_1)} \left(\dfrac{\theta_{\text{tip}} L_{\text{dw}}}{w_{\text{c}}}\right)^{c_1}\right]}{(1+\lambda L_{\text{dw}})} & u_{\text{z,cr}} \le u_{\text{z, max}} \le w_{\text{c}} + u_{\text{z,cr}} \\ \dfrac{f_{\text{ct}} b_{\text{n}} L_{\text{dw}}}{2(1-\alpha)\lambda(1+\lambda L_{\text{dw}})} + \dfrac{f_{\text{ct}} b_{\text{n}} \left[\dfrac{c_1 L_{\text{dw}} w_{\text{c}}}{(1+c_1)\theta_{\text{tip}}} - \dfrac{c_1 w_{\text{c}}^2}{2\left(2+c_1\right)\theta_{\text{tip}}^2}\right]}{1+\lambda L_{\text{dw}}} & u_{\text{z, max}} > w_{\text{c}} + u_{\text{z,cr}} \end{cases} \tag{28}$$

Depending on vertical displacement $u_{\text{z,max}}$ at the crack end, two different equations can be derived. The detailed derivation procedure can be found in Appendix A. On the right-hand side of Eq. (28), the variables L_{dw} and θ_{tip} can be represented by M_{tip} and $u_{\text{z,max}}$ using the Eqs. (21) and (27). By substituting Eqs. (21) and (27) into Eq. (28), only two unknowns remain in this equation, which are M_{tip} and $u_{\text{z,max}}$ To solve the equation, $u_{\text{z,max}}$ is used as an input parameter, and then, M_{tip} can be obtained by implementing a numerical method, for instance, the bisection method. With a calculated M_{tip}, the dowel resistance V_{dw} can be obtained using Eq. (24).

2.3. Unstable dowel cracking

The last stage of the dowel fracturing process is unstable dowel cracking. In this stage, the propagation of the dowel crack becomes unstable. This is often observed in shear tests of members without shear reinforcement, and some of the dowel tests [15,19,24]. To demonstrate this phenomenon, an example is given by implementing the model with the material properties of Specimen Beam 2.2 in [15]. The relationships between the input vertical displacement $u_{\text{z,max}}$ and M_{tip}, V_{tip} are shown in Fig. 6, in which M_{tip} increases while V_{tip} decreases as the vertical displacement $u_{\text{z,max}}$ increases. Without any constraint condition, the value of V_{tip} can be even lower than zero, it suggests that at certain vertical displacement, the required shear force at the crack tip is negative, which means the cracking is fully driven by the moment applied to the crack tip M_{tip} from that point on. Under that situation, the dowel splitting crack can propagate further without any additional vertical force at the free end until the boundary conditions change, for instance, the crack reaches the support. This stage is defined as unstable cracking in this paper.

The moment at the crack tip just before the unstable cracking occurs is in fact the maximum allowable moment. It is defined by $M_{\text{tip,max}}$ and can be derived using Eq. (19) and $V_{\text{tip}} = 0$.

$$M_{\text{tip, max}} = \frac{f_{\text{ct}} b_{\text{n}}}{2(1-\alpha)\lambda^2} \tag{29}$$

Substituting Eqs. (21) and (29) into Eq. (28), the critical dowel crack length $L_{\text{dw,crit}}$ and the corresponding critical vertical displacement at the free end $u_{\text{z,crit}}$, before the unstable dowel cracking occurs, can be obtained. When $u_{\text{z,crit}} \ge w_{\text{c}} + u_{\text{z,cr}}$, in this case, the maximum crack width w_{max} is larger than the characteristics crack width w_{c} defined in Eq. (22) for transferring the residual tensile stress. Then, an analytical solution of both $L_{\text{dw,crit}}$ and $u_{\text{z,crit}}$ can be derived as follows:

$$L_{\text{dw,crit}} = \frac{(1+c_1) f_{\text{ct}} b_{\text{n}}}{(1-\alpha)^2 c_1 w_{\text{c}} \lambda k n} + \frac{(1-\alpha)(1+c_1) w_{\text{c}} k n}{4(2+c_1)\lambda f_{\text{ct}} b_{\text{n}}} \tag{30}$$

$$u_{\text{z,crit}} = \frac{2(1+c_1) f_{\text{ct}}^2 b_{\text{n}}^2}{(1-\alpha)^3 c_1 w_{\text{c}} k^2 n^2} + \frac{(1+c_1) w_{\text{c}}}{2(2+c_1)} + \frac{f_{\text{ct}} b_{\text{n}}}{(1-\alpha) k n} \tag{31}$$

Regarding the situation when $u_{\text{z,crit}} < w_{\text{c}} + u_{\text{z,cr}}$, the corresponding maximum dowel crack length $L_{\text{dw,crit}}$ and the vertical displacement at the free end $u_{\text{z,crit}}$ can be calculated by implementing a numerical method. The first scenario is in most cases.

2.4. Summary and solution flowchart

The solution flowchart of the proposed model can be seen in Fig. 7. This calculation procedure generates the full relationship between vertical displacement at the free end u_{z} and dowel resistance V_{dw}. Taking Beam 2.2 in [15] as an example again, Fig. 8(a) shows the full shear force-displacement curve calculated from the proposed model compared with the measurement reported in [15]. The model proposed in this

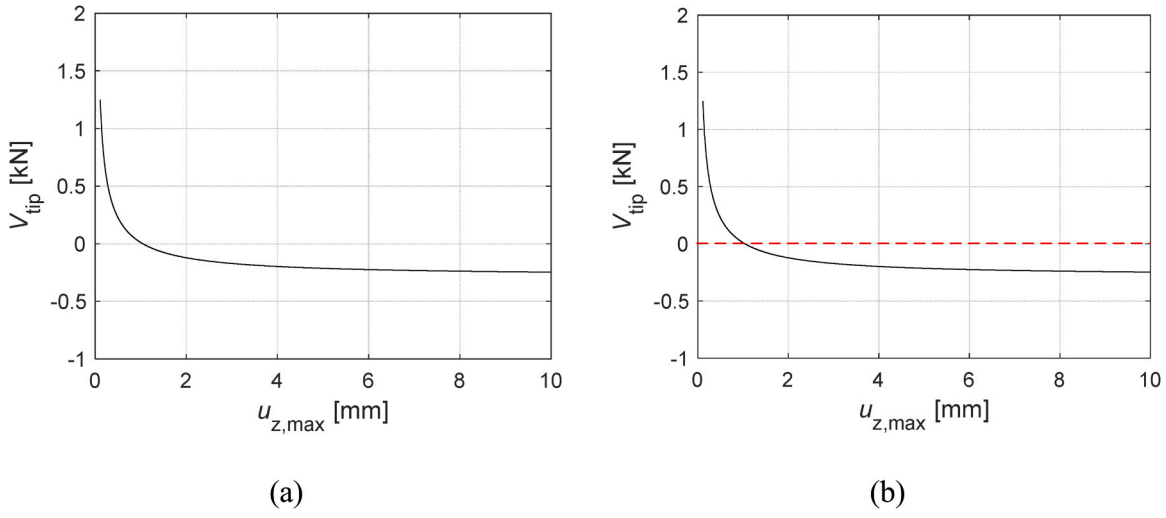

Fig. 6. Calculation results using the proposed model: (a) relationship between $u_{\text{z,max}}$ and M_{tip}; (b) relationship between $u_{\text{z,max}}$ and V_{tip}.

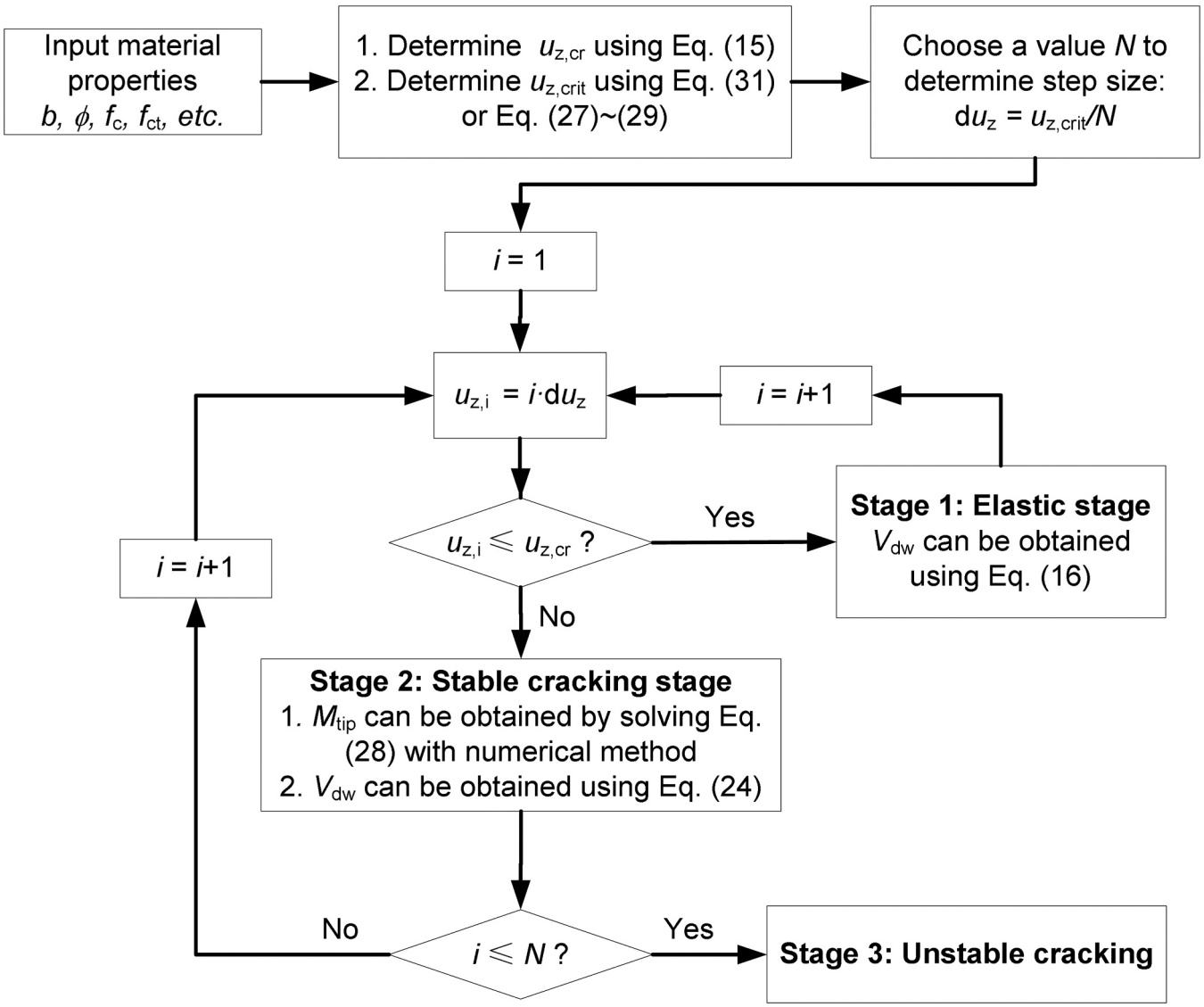

Fig. 7. Solution flowchart for the proposed model.

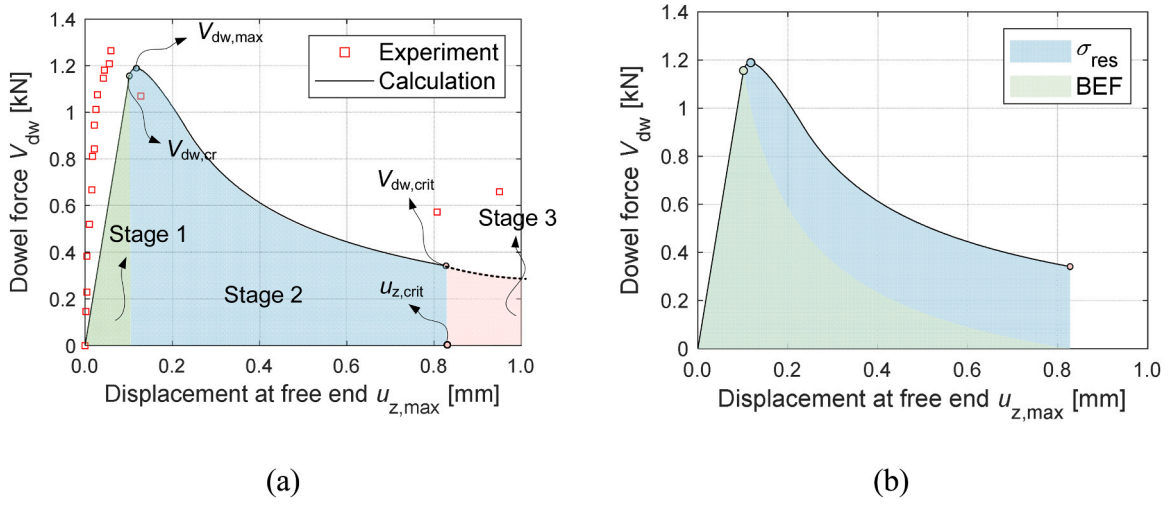

Fig. 8. The displacement versus force curve of Beam 2.2: (a) comparison against Beam 2.2 from [15] (b) contributions from different mechanisms.

paper can capture both the maximum dowel resistance and the post-peak behaviour. Fig. 8(b) shows the contributions made by two mechanisms during the full dowel splitting cracking evolution. After reaching the cracking load $V_{dw,cr}$, the contribution from the BEF starts to decrease since part of the transversal tensile stress $\sigma_{ct,max}$ is induced by the moment at the crack tip. On the other hand, the contribution of the residual tensile strength starts to increase and stabilises as the crack opening increases. Therefore, the characteristics of the stable dowel cracking stage are determined by both the concrete tensile behaviour and the rebar configuration. When the contribution from the BEF fully diminishes, the unstable cracking starts because the crack opening is fully driven by the moment acted at the crack tip. A more extensive validation of the proposed model can be seen in Chapter. 3.

2.5. Simplified equation for the maximum dowel force

It should be noted that there is no analytical equation for the maximum dowel force $V_{dw,max}$ in the proposed model. However, as shown in, Fig. 8(a), the maximum dowel force $V_{dw,max}$ is very close to the cracking dowel force $V_{dw,cr}$, which coincides with the observations for conventional concrete in [8]. If the differences between $V_{dw,cr}$ and $V_{dw,max}$ are ignored, a simplified expression for $V_{dw,max}$ can be derived by substituting Eqs. (5) and (6) into Eq. (14) and setting Young's modulus of steel $E_s = 210$ GPa and $c_f = 0.6$.

$$V_{dw,\,max} \approx V_{dw,cr} = 2.4\beta b_n \phi^{\frac{11}{12}} f_{ct} f_c^{-\frac{1}{8}} \tag{32}$$

where $\beta = 1/(1\text{-}\alpha_{crit})$ is a factor to consider the influence of concrete cover and α_{crit} can be calculated using Eq. (13).

If a relationship between concrete tensile strength f_{ct} and compressive strength f_c is adopted, Eq. (32) can be further simplified, which can be found in Section 4.3.

3. Model verification

3.1. Maximum dowel force

To evaluate the proposed model, in total 53 specimens were collected from the literature [8,15,19,24]. A detailed list of the corresponding data is given in Appendix B. Considering the assumptions of the model, only test results using the block-type testing setup, indicated by Fig. 1(a), and with one layer of rebar are selected in the database.

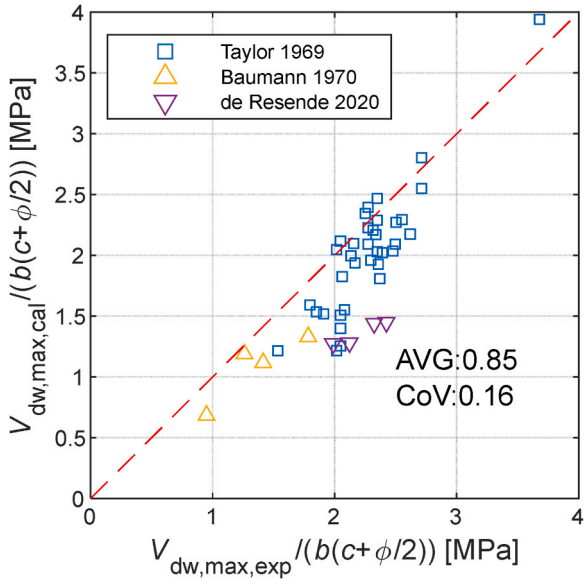

Fig. 9. Comparison between calculated results and experimental data.

Moreover, for consistency, only the experiments with reported tensile splitting strength were used in the comparison, which resulted in 44 specimens. However, a more extensive discussion on the influence of selected tensile strength will be discussed in Section 4.3. Fig. 9 describes the comparison between the results calculated by the proposed model and the experimental results. The maximum dowel force $V_{dw,max}$ is normalized by using the area underneath the centre of the rebar so that the data is easier to compare within the range. Overall the proposed model slightly underestimates the maximum dowel force but with reasonable accuracy. The average value of the ratio between $V_{dw,max,cal}$ and $V_{dw,max,exp}$ is 0.85 and the coefficient of variation (CoV) is 0.16. On the other hand, it should be noted that most of the available experiments on dowel splitting tests were conducted on small-size specimens and only the maximum dowel force was recorded. More experiments with a realistic size on dowel splitting and more refined measurement techniques are recommended in future work.

3.2. Displacement versus force curve

The older experiments usually only reported the maximum dowel force. However, the full load-deformation relationship is very crucial for a better understanding of the dowel action mechanism. Therefore, four specimens were collected from the recent work published by de Resende [8] besides the comparison of Beam 2.2 shown in Fig. 8. The letter D in the legend stands for the experiments performed with additional measurement techniques according to [8].

Fig. 10 shows the comparison between model prediction and experimental data. Using the mechanical properties provided by [8], the proposed model underestimates the experimental results, while the tendency of softening behaviour is very similar. The underestimation can be partly attributed to the scatter of the concrete tensile strength. For the specimens with 12.5 mm rebar, as shown in Fig. 10 (a), the calculated vertical displacement for unstable cracking $u_{z,crit}$ is comparable to the last recording point of the experimental data, although the reasons for terminating the test were not reported in [8]. For the specimens with 16 mm rebar, as shown in Fig. 10 (b), a stabilized stage can be observed in the last part of the curve and the vertical displacement of the starting point of the stabilized stage is comparable to the calculated vertical displacement for unstable cracking.

4. Discussions

4.1. Novelty of the proposed model

In literature there are several different models based on BEF theory that can describe the dowel action. There are two major differences between the proposed model and these models. The fundamental difference between the models in literature and the proposed model is that most models in literature are plasticity-based models and the equilibrium conditions are not considered after the occurrence of the cracking. Fig. 11 (a) shows the assumed concrete tensile stress distribution along the rebar using BEF theory. Along the assumed characteristic length L_0 the stress level of concrete is constant, accordingly the maximum dowel force is:

$$V_{dw,\,max} = b_n f_{ct} L_0 \tag{33}$$

The value of L_0 is back-calibrated by the experimental data or related to the inflexion point of concrete tensile stress distribution [20,22,24]. This assumption is clearly different from the concrete post-crack behaviour generally observed in reality. Such a model is therefore not capable of predicting dowel action responses after the formation of dowel crack.

The proposed model, on the contrary, considers the residual tensile strength σ_{res} of concrete after cracking, which allows us to derive an expression of the full response of the dowel cracking process in terms of vertical displacement and dowel force. As an important step in the

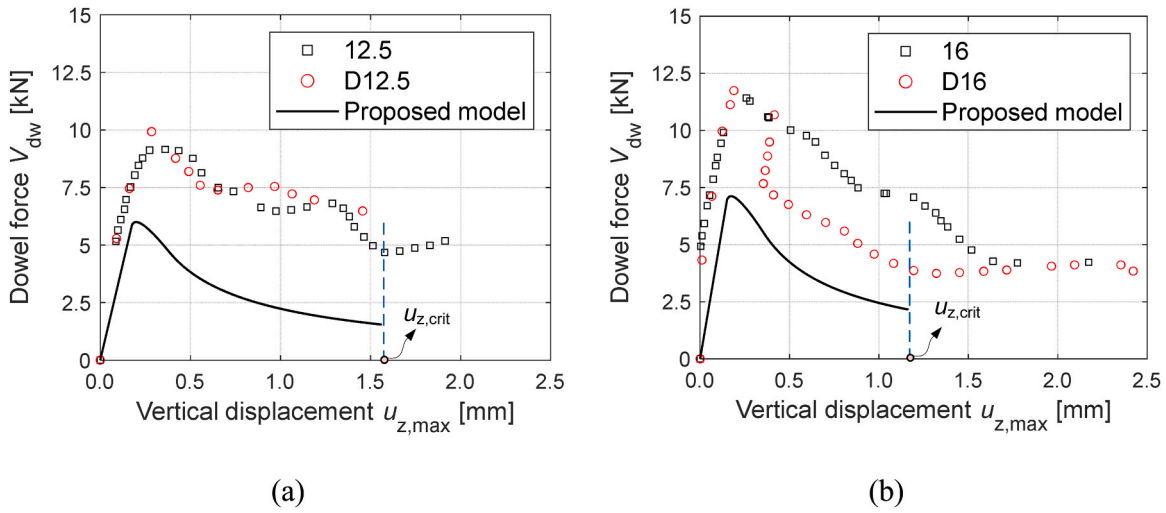

Fig. 10. Comparison of full displacement versus force curve between calculated results and experimental data: (a) specimens with rebar of 12.5 mm (b) specimens with rebar of 16 mm.

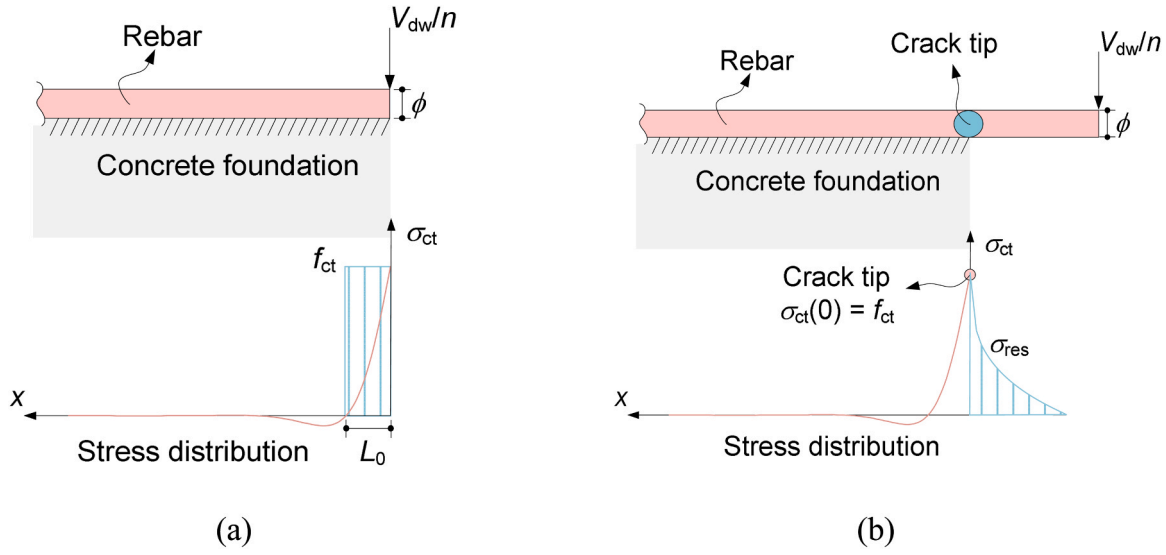

Fig. 11. Differences between the existing models and proposed model: (a) existing models (b) proposed model.

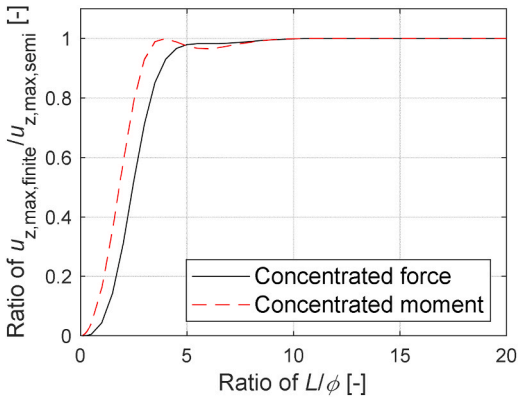

Fig. 12. Differences between the finite beam solutions and semi-infinite solutions.

derivation, the proposed model also considers the additional moment M_{tip} acted at the crack tip after dowel cracking. This is essential to model the softening behaviour after the peak load and especially the unstable cracking stage of dowel cracking. Therefore, the proposed model can predict the full load-displacement response for the propagation of dowel splitting crack. It has the potential to be further incorporated into the existing kinematic-based shear models, which may lead to new insight into the shear failure of beams without shear reinforcement.

4.2. *Influence of the total length*

In Section 2.1, the analytical solutions for a semi-infinite beam in BEF theory are used for the sake of simplicity in formulation. The impact of this assumption is examined in this section. The analytical solutions for both a finite beam and a semi-infinite beam under a unit concentrated load and moment are compared. The comparison uses the mechanical properties based on the data of Specimen 12.5 reported in [8]. In Fig. 12 (a), the differences between the two types of models in terms of the maximum vertical displacement under concentrated load as well as moment are compared. It is clear that when the ratio between the

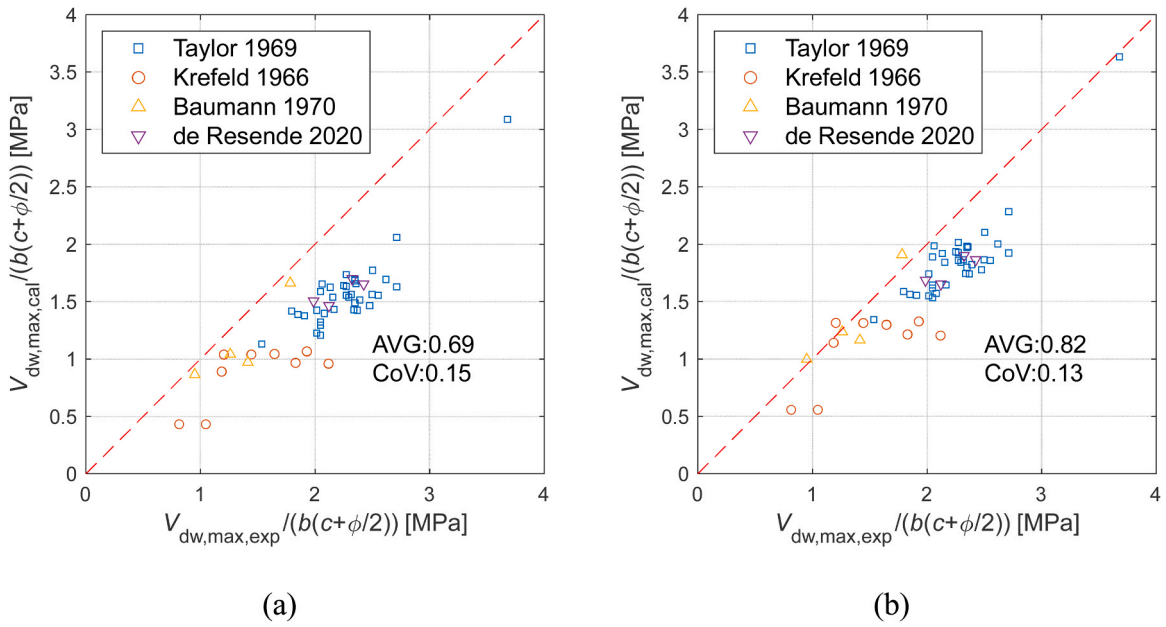

Fig. 13. Comparison between calculated results and experimental data: (a) using tensile strength based on *fib* Model Code 2010 [30]; (b) using splitting tensile strength based on Eq. (34) proposed in [31].

beam length L and rebar diameter ϕ is larger than 5, the difference between the two solutions is very limited. On the other hand, when the ratio is smaller than 5, using the finite beam solutions can give a smaller vertical displacement. Then, according to Eq. (19), the maximum transversal tensile stress in the concrete is smaller. As a consequence, a large load is needed to induce the dowel cracking. Therefore, a higher maximum dowel force is expected, which also coincides with the conclusion drawn by Krefeld and Thurston [19]. In most cases, the dowel splitting in a normal reinforced beam occurs under the condition of L/ϕ larger than 5.

4.3. Influence of the concrete tensile strength

In Section 3.1, the comparison between the experimental data and the calculations shows a relatively high scatter, which can be attributed to the scatter in the concrete tensile strength by nature. A parametric study is performed using two different concrete tensile strengths. They are both calculated using the concrete compressive strength, which was reported for all specimens. Therefore, all 53 specimens are included in the following comparisons. For the comparison shown in Fig. 13(a), the direct tensile strength f_{ct} is used and the value is determined based on the compressive strength f_c using the relationship proposed by the *fib* Model Code 2010 [30]. For the comparison shown in Fig. 13(b), the splitting tensile strength $f_{ct,sp}$ is used and the value is determined by Eq. (34) proposed by Bentz et al. [31]. The comparison shows that using the tensile strength translated from the compressive strength can reduce the scatter in the comparison, which means a smaller CoV can be obtained. However, using tensile strength f_{ct} can lead to a relatively conservative prediction with an average ratio of 0.69. If the splitting tensile strength $f_{ct,sp}$ is used, a lower CoV of 0.13 and a higher average value of 0.82 can be obtained. Therefore, it is suggested to use splitting tensile strength $f_{ct,sp}$ to calculate the maximum dowel force:

$$f_{ct,sp} = 0.62\sqrt{f_c} \tag{34}$$

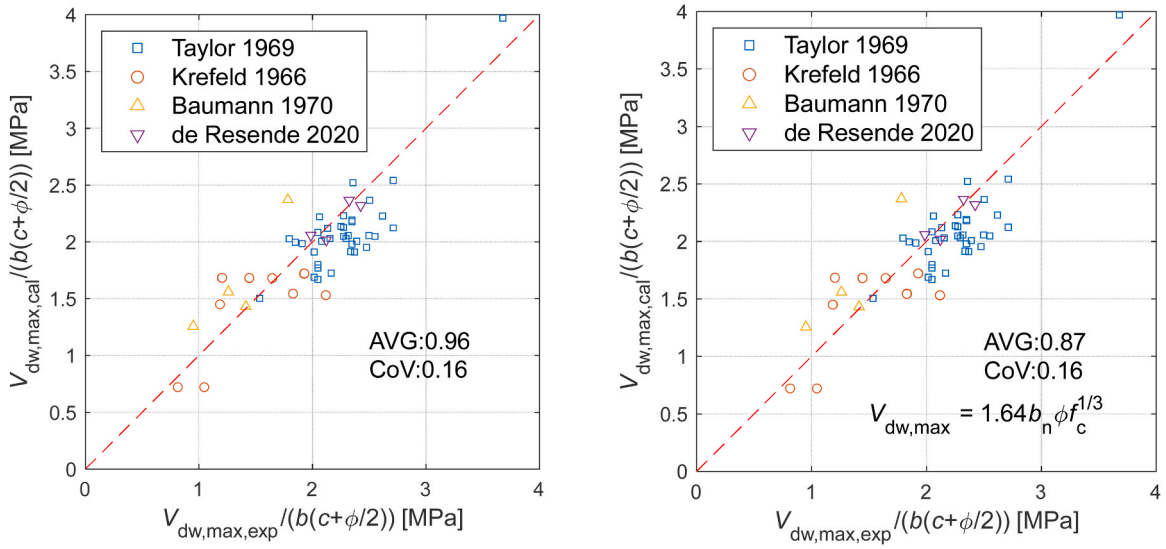

Fig. 14. Comparison between calculated results and experimental data: (a) simplified equation; (b) equation proposed by Baumann & Rüsch [24].

where $f_{ct,sp}$ is in MPa and f_c is in MPa.

In Section 2.5, a simplified equation for the maximum dowel force based on the proposed model was proposed. By combining Eq. (34) and Eq. (32), a more compact equation can be derived:

$$V_{dw,\,max} = 2.4\beta b_n \phi^{\frac{11}{12}} f_{ct} f_c^{-\frac{1}{8}} \approx 1.5\beta b_n \phi f_c^{\frac{3}{8}} \tag{35}$$

where b_n is in mm, ϕ is in mm and f_c is in MPa.

The comparison against experimental data using the simplified equation can be seen in Fig. 14(a). Although The form of Eq. (35) is very similar to the equation proposed by Baumann & Rüsch [24], which can be found in Fig. 14(b), the proposed equation is derived analytically without any calibrations. As a comparison, the results calculated by their equation are also shown in Fig. 14(b). Compared to their equation, the proposed simplified equation can achieve the same level of CoV and higher accuracy with an average value of 0.96. The improvement of the accuracy can be attributed to the consideration of the factor β, which can include the influence of the concrete cover.

4.4. Influence of the tensile force in the reinforcement

As a limitation of the proposed model, the influence of the tensile force of the reinforcement is not considered in this model yet. It is inevitable to have tensile force in the reinforcement of a beam subject to bending. The difference of the tensile forces in the reinforcement at different cross sections will inevitably result in bond stresses between concrete and the reinforcement, which will affect the stress conditions of concrete around the reinforcement. However, there is no consensus regarding the influence of axial force on dowel action among the scientific community yet. According to Autrup et al. [7], the existence of high axial force, which is around 0.6 times the yielding strength of rebar, can highly affect the dowel action responses. Houde and Mirza [32] concluded that the dowel action capacity was not influenced by the axial force when the axial stresses were less than the yielding strength of the rebar. Jimenez et al. [33] observed a slight decrease in dowel capacity when the axial stress was around 275 MPa to 400 MPa. For the sake of simplicity in formulation, the axial force in reinforcement is not considered in this paper. Therefore, it shall be noted that the proposed model is more suitable for cases where the axial force is small compared to the yield strength of the rebar. For cases where the axial force is comparable to the yield strength, readers can refer to the model proposed by Mihaylov [34] or Autrup [7].

5. Conclusions

This paper proposes a mechanical model which is analytically derived based on the beam on elastic foundation theory and fracture mechanics. The main findings of the paper can be summarized as follows:

- By introducing the residual tensile strength of concrete after cracking, the model can capture the post-peak softening behaviour of dowel action, which is validated by experimental results reported in literature.
- The proposed model theoretically proves and explains the occurrence of unstable propagation in dowel action. A closed-form expression for the maximum vertical displacement and dowel crack length at the onset of unstable cracking is derived.
- When compared with experimental data obtained from the literature, the model can predict both the maximum dowel force and shear displacement with reasonable accuracy.
- A simplified analytical expression of the maximum dowel force is suggested with pleasing accuracy.

CRediT authorship contribution statement

Max A.N. Hendriks: Writing – review & editing, Supervision, Methodology, Conceptualization. **Yuguang Yang:** Writing – review & editing, Supervision, Project administration, Methodology, Conceptualization. **Jiandong Lu:** Writing – original draft, Visualization, Validation, Methodology, Investigation, Formal analysis, Data curation, Conceptualization.

Declaration of Competing Interest

The authors declare that they have no known competing financial interests or personal relationships that could have appeared to influence the work reported in this paper.

Data Availability

Data will be made available on request.

Acknowledgement

The author Jiandong Lu would like to acknowledge the funding support from China Scholarship Council (CSC) under the grant CSC No. 202106150029.

Appendix A. Derivation of closed-form analytical equation for M_{tip}

Substituting Eq. (23) into Eq. (24), the following equation can be obtained.

$$M_{tip} - V_{tip}L_{dw} = b_n L_{dw}\int_0^{L_{dw}} \sigma_{res}\mathrm{d}x - b_n\int_0^{L_{dw}} \sigma_{res} l x \mathrm{d}x \tag{A.1}$$

Then, substituting Eq. (19) into Eq. (A.1), a closed-form equation of M_{tip} can be obtained after simplification.

$$\left(1+\lambda L_{dw}\right)M_{tip} = \frac{b_n f_{ct} L_{dw}}{2(1-\alpha)\lambda} + b_n L_{dw}\int_0^{L_{dw}} \sigma_{res}\mathrm{d}x - b_n\int_0^{L_{dw}} \sigma_{res} x \mathrm{d}x \tag{A.2}$$

For the first integral on the right-hand side, two situations can be obtained depending on whether the maximum crack width w_{max} exceeds w_c that can transfer the residual strength.

$$b_n L_{dw} \int_0^{L_{dw}} \sigma_{res} dx = f_{ct} \int_0^{L_{dw}} \left[1 - \left(\frac{w}{w_c}\right)^{c1}\right] dx$$

$$= \begin{cases} b_n f_{ct} L_{dw}^2 \left[1 - \frac{1}{c_1+1}\left(\frac{\theta_{tip} L_{dw}}{w_c}\right)^{c_1}\right] & w_{max} < w_c \\ b_n f_{ct} L_{dw} \frac{w_c}{\theta_{tip}} \frac{c_1}{c_1+1} & w_{max} \geq w_c \end{cases} \quad (A.3)$$

For the second integral, it can be simplified using the same approach.

$$b_n \int_0^{L_{dw}} \sigma_{res} x dx = f_{ct} \int_0^{L_{dw}} l \left[1 - \left(\frac{w}{w_c}\right)^{c1}\right] dx$$

$$= \begin{cases} b_n f_{ct} L_{dw}^2 \left[\frac{1}{2} - \frac{1}{c_1+2}\left(\frac{\theta_{tip} L_{dw}}{w_c}\right)^{c_1}\right] & w_{max} < w_c \\ b_n f_{ct} \left(\frac{w_c}{\theta_{tip}}\right)^2 \frac{c_1}{2(c_1+2)} & w_{max} \geq w_c \end{cases} \quad (A.4)$$

Finally, substituting Eqs. (A.3) and (A.4) into Eq. (A.2) can result in the governing equation Eq. (28). The governing equation Eq. (28) can be solved by numerical methods such as the bisection method.

Appendix B. Database of dowel action from literature

Note:

1. The splitting tensile strength listed in the table were collected from the literature;
2. The calculated results were obtained based on the translated splitting tensile strength using Eq. (34). Therefore, the calculated results in the table correspond to the results in Fig. 13(b).

No.	name	source	L [mm]	h [mm]	b [mm]	c [mm]	ϕ [mm]	n [-]	f_c [MPa]	$f_{ct,sp}$ [Mpa]	$V_{dw,max,exp}$ [kN]	$V_{dw,max,cal}$ [kN]	$V_{dw,max,cal}/V_{dw,max,exp}$ [-]
1	Beam 1.1	Taylor 1969[15]	87.00	87.00	44.00	7.60	6.00	2.00	18.20	2.76	1.11	0.81	0.73
2	Beam 1.2		87.00	87.00	44.00	7.60	6.00	2.00	24.00	3.17	1.00	0.90	0.90
3	Beam 1.3		87.00	87.00	44.00	7.60	6.00	2.00	21.90	3.31	1.06	0.87	0.82
4	Beam 1.4		87.00	87.00	44.00	7.60	6.00	2.00	21.90	3.66	1.19	0.87	0.73
5	Beam 2.1		174.00	87.00	44.00	7.60	6.00	2.00	21.40	3.07	1.07	0.86	0.80
6	Beam 2.2		174.00	87.00	44.00	7.60	6.00	2.00	24.10	4.14	1.27	0.90	0.71
7	Beam 2.3		174.00	87.00	44.00	7.60	6.00	2.00	19.30	3.17	1.16	0.83	0.71
8	Beam 2.4		174.00	87.00	44.00	7.60	6.00	2.00	20.70	3.17	1.12	0.85	0.76
9	Beam 3		174.00	87.00	44.00	7.60	6.00	2.00	18.30	3.38	1.09	0.81	0.75
10	Beam 4		174.00	87.00	44.00	7.60	6.00	2.00	22.10	3.31	1.17	0.87	0.74
11	Beam 5		174.00	87.00	44.00	7.60	6.00	2.00	18.20	3.17	0.94	0.81	0.86
12	Beam 6		174.00	87.00	44.00	7.60	6.00	2.00	38.90	4.83	1.27	1.06	0.84
13	Beam 7		130.00	87.00	44.00	7.60	6.00	2.00	22.90	3.37	0.96	0.88	0.92
14	Beam 8		174.00	87.00	44.00	7.60	6.00	2.00	27.50	3.93	1.06	0.94	0.89
15	Beam 9		218.00	87.00	44.00	7.60	6.00	2.00	24.20	3.58	1.06	0.90	0.85
16	Beam 10		263.00	87.00	44.00	7.60	6.00	2.00	24.50	3.79	1.05	0.90	0.86
17	Beam 11		174.00	87.00	44.00	7.60	6.00	2.00	21.40	3.31	1.01	0.86	0.85
18	Beam 12		174.00	87.00	44.00	7.60	6.00	2.00	25.80	4.03	1.10	0.92	0.84
19	Beam 13		174.00	87.00	44.00	7.60	6.00	2.00	22.10	3.51	1.08	0.87	0.81
20	Beam 14		174.00	87.00	44.00	2.50	6.00	2.00	24.10	3.34	0.89	0.88	0.99
21	Beam 15		174.00	87.00	44.00	7.60	6.00	2.00	26.20	3.72	1.10	0.92	0.84
22	Beam 16		174.00	87.00	44.00	12.70	6.00	2.00	24.10	2.72	1.06	0.93	0.88
23	Beam 17		174.00	87.00	44.00	7.60	6.00	1.00	24.10	2.96	1.10	0.92	0.84
24	Beam 18		174.00	87.00	44.00	7.60	6.00	2.00	20.00	3.17	1.10	0.84	0.76
25	Beam 19		174.00	87.00	44.00	7.60	6.00	3.00	24.10	3.72	1.01	0.77	0.76
26	Beam 20		174.00	87.00	49.00	7.60	6.00	2.00	24.80	3.38	1.36	1.04	0.76
27	Beam 21		174.00	87.00	54.00	7.60	6.00	2.00	22.70	2.69	1.18	1.14	0.96
28	Beam 22		174.00	87.00	59.00	7.60	6.00	2.00	25.20	3.38	1.57	1.31	0.84
29	Beam 25		174.00	87.00	44.00	7.60	6.00	2.00	13.10	1.65	0.94	0.72	0.77

(continued on next page)

(*continued*)

No.	name	source	L [mm]	h [mm]	b [mm]	c [mm]	ϕ [mm]	n [-]	f_c [MPa]	$f_{ct,sp}$ [Mpa]	$V_{dw,max,exp}$ [kN]	$V_{dw,max,cal}$ [kN]	$V_{dw,max,cal}/V_{dw,max,exp}$ [-]
30	Beam 26		174.00	87.00	44.00	7.60	6.00	2.00	14.80	2.00	0.96	0.75	0.79
31	Beam 27		174.00	87.00	44.00	7.60	6.00	2.00	15.50	2.20	0.96	0.77	0.80
32	Beam 28		174.00	87.00	44.00	7.60	6.00	2.00	12.70	1.72	0.96	0.72	0.74
33	P1		609.00	304.50	154.00	38.16	22.00	2.00	38.60	3.86	13.60	12.02	0.88
34	P2		609.00	304.50	154.00	38.16	22.00	2.00	37.00	3.70	14.00	11.83	0.85
35	P3		609.00	304.50	154.00	38.16	22.00	2.00	37.50	3.75	15.75	11.89	0.76
36	P4		609.00	304.50	154.00	38.16	22.00	2.00	36.50	3.65	14.45	11.78	0.81
37	DA-2	Krefeld & Thurston 1966	304.80	304.8	152.40	38.16	22.23	2.00	18.28		15.90	9.04	0.57
38	DA-3	[19]	457.20	304.8	155.45	38.16	22.23	2.00	18.28		14.01	9.29	0.66
39	DA-1		609.60	304.8	152.40	38.16	22.23	2.00	15.79		8.90	8.57	0.96
40	DA-6		304.80	304.8	203.20	38.16	22.23	2.00	18.07		14.46	13.15	0.91
41	DA-7		762.00	304.8	206.25	38.16	22.23	2.00	17.93		12.23	13.36	1.09
42	DA-9		304.80	381	152.40	114.36	22.23	2.00	16.48		20.02	10.66	0.53
43	DA-8		609.60	381	152.40	114.36	22.23	2.00	16.48		15.57	10.66	0.68
44	DA-5		304.80	304.8	158.75	38.00	28.65	2.00	19.10		16.01	11.02	0.69
45	DA-4		609.60	304.8	152.40	38.00	28.65	2.00	19.10		13.12	10.35	0.79
46	15	Baumann & Rüsch 1970	450.00	320	110.00	20	20.00	2.00	31.22	2.29	5.88	6.30	1.07
47	8	[24]	450.00	320	110.00	33	16.00	2.00	24.01	2.90	6.37	5.26	0.83
48	11		450.00	320	110.00	33	26.00	2.00	24.01	2.90	6.37	6.26	0.98
49	16		450.00	320	110.00	51	20.00	2.00	31.22	2.29	6.37	6.70	1.05
50	12.5	de Resende et al. 2020[8]	360.00	250.00	150.00	25.00	12.50	2.00	38.70	2.88	9.31	7.90	0.85
51	D12.5		360.00	250.00	150.00	25.00	12.50	2.00	36.70	2.88	9.94	7.75	0.78
52	16		360.00	250.00	150.00	25.00	16.00	2.00	38.70	2.88	11.50	9.41	0.82
53	D16		360.00	250.00	150.00	25.00	16.00	2.00	36.70	2.88	12.00	9.23	0.77
												AVG	0.82
												CoV	0.13

References

[1] Marí A, et al. Shear-flexural strength mechanical model for the design and assessment of reinforced concrete beams. Struct Infrastruct Eng 2015;11(11):1399–419.

[2] Cavagnis F, Ruiz MF, Muttoni A. A mechanical model for failures in shear of members without transverse reinforcement based on development of a critical shear crack. Eng Struct 2018;157:300–15.

[3] Campana S, et al. Analysis of shear-transfer actions on one-way RC members based on measured cracking pattern and failure kinematics. Mag Concr Res 2013;65(6):386–404.

[4] Huber P, Huber T, Kollegger J. Investigation of the shear behavior of RC beams on the basis of measured crack kinematics. Eng Struct 2016;113:41–58.

[5] Classen M. Shear Crack Propagation Theory (SCPT)–The mechanical solution to the riddle of shear in RC members without shear reinforcement. Eng Struct 2020;210:110207.

[6] Yang, Y., Shear Behaviour of Reinforced Concrete Members without Shear Reinforcement, in Delft University of Technology. 2014.

[7] Autrup F, Jørgensen HB, Hoang LC. Dowel action of the tensile reinforcement in RC beams without shear reinforcement: novel experimental investigation and mechanical modelling. Eng Struct 2023;279.

[8] de Resende TL, Cardoso DC, Shehata LC. Influence of steel fibers on the dowel action of RC beams without stirrups. Eng Struct 2020;221:111044.

[9] Yang Y, Walraven J, Uijl Jd. Shear behavior of reinforced concrete beams without transverse reinforcement based on critical shear displacement. J Struct Eng 2017;143(1):04016146.

[10] Friberg BF. Design of dowels in transverse joints of concrete pavements. Trans Am Soc Civ Eng 1940;105(1):1076–95.

[11] Acharya DN, Kemp K. Significance of dowel forces on the shear failure of rectangular reinforced concrete beams without web reinforcement. Acids J Proc 1965;62(10).

[12] Muttoni A, Fernández Ruiz M. Shear strength of members without transverse reinforcement as function of critical shear crack width. Acids Struct J 2008;105:163–72.

[13] Cavagnis F, Fernández Ruiz M, Muttoni A. A mechanical model for failures in shear of members without transverse reinforcement based on development of a critical shear crack. Eng Struct 2018;157:300–15.

[14] Reineck K-H. Ultimate shear force of structural concrete members without transverse reinforcement derived from a mechanical model (SP-885). Struct J 1991;88(5):592–602.

[15] Taylor, H., Investigation of the dowel shear forces carried by the tensile steel in reinforced concrete beams. 1969.

[16] Chana P. Investigation of the mechanism of shear failure of reinforced concrete beams. Mag Concr Res 1987;39(141):196–204.

[17] Kim W, White RN. Hypothesis for localized horizontal shearing failure mechanism of slender RC beams. J Struct Eng 1999;125(10):1126–35.

[18] Fischer J, Koenig G. Mechanical model for diagonal tension failure. CEB Comité Euro international du Béton. Bulletin 1997;237:231–46.

[19] Krefeld WJ, Thurston CW. Contribution of longitudinal steel to shear resistance of reinforced concrete beams. *J Proc* 1966.

[20] Vintzēleou E, Tassios T. Mathematical models for dowel action under monotonic and cyclic conditions. Mag Concr Res 1986;38(134):13–22.

[21] Fenwick R, Paulay T. Mechanisms of shear resistance of concrete beams. J Struct Div 1968;94(10):2325–50.

[22] Soroushian P. Behavior of bars in dowel action against concrete cover. Struct J 1987;84(2):170–6.

[23] Soroushian P, Obaseki K, Rojas MC. Bearing strength and stiffness of concrete under reinforcing bars. Mater J 1987;84(3):179–84.

[24] Baumann T, Rüsch H. Tests studying the dowel action of the flexural tensile reinforcement of reinforced concrete beams. Versuche zum Studium der Verdubelungswirkung der Biegezugbewehrung eines Stahlbetonbalkens. Berlin: Wilhelm Ernst und Sohn,; 1970. p. 42–82.

[25] Muttoni A. Punching shear strength of reinforced concrete slabs without transverse reinforcement. Acids Struct J 2008;105:440–50.

[26] Cavagnis F, et al. Shear strength of members without transverse reinforcement based on development of critical shear crack. Acids Struct J 2020;117(1).

[27] Marcus H. Load carrying capacity of dowels at transverse pavement joints. *J Proc* 1951.

[28] Hetényi M. Beams on Elastic Foundation: Theory with Applications in the Fields of Civil and Mechanical Engineering. University of Michigan Press,; 1946.

[29] Reinhardt HW. Fracture mechanics of an elastic softening material like concrete. HERON 1984;29(2):1984.

[30] Fédération Internationale du Béton (fib), fib Model Code for Concrete Structures 2010. 2013, Ernst & Sohn. p. 434.

[31] Bentz, D.P., et al., *Influence of aggregate characteristics on concrete performance*. 2017, US Department of Commerce, National Institute of Standards and Technology.

[32] Houde J, Mirza MS. A finite element analysis of shear strength of reinforced concrete beams. Spec Publ 1974;42:103–28.

[33] Jimenez R, White R, Gergely P. Bond and dowel capacities of reinforced concrete. *J Proc* 1979.

[34] Mihaylov B. Five-spring model for complete shear behaviour of deep beams. Struct Concr 2015;16(1):71–83.